ChemComm

Cobalt Phosphide (Co_2P) Encapsulated in Nitrogen-rich Hollow Carbon Nanocages with Fast Rate Potassium Ion Storage

Journal:	*ChemComm*
Manuscript ID	CC-COM-10-2020-007123
Article Type:	Communication

COMMUNICATION

Cobalt Phosphide (Co_2P) Encapsulated in Nitrogen-rich Hollow Carbon Nanocages with Fast Rate Potassium Ion Storage

Debanjan Das,[a] Debasish Sarkar,*[b] Sudhan Nagarajan,[c] and David Mitlin*[d]

Received 00th January 20xx,
Accepted 00th January 20xx

DOI: 10.1039/x0xx00000x

We synthesized Co_2P nanoparticles encapsulated N-doped carbon nanocages through one-step carbonization-phosphidation of ZIF-67. As potassium ion battery (KIB, PIB) anodes Co_2P@NCCs displays state-of-the-art electrochemical performance, including most favorable fast charge characteristics reported. The single-nanometer thick carbon cage yields rapid solid-state K-ion diffusion and prevents aggregation/pulverization of 40 nm cobalt phosphide.

Sodium and potassium ion storage are being considered as an alternative to lithium due to their natural abundance and low cost. The standard hydrogen potential of K (-2.94 vs E^0) is quite close to that of Li (-3.04 vs E^0), which in principle allows for high voltage potassium ion batteries (KIBs). A key challenge with K is to find suitable anodes that could withstand the volume changes caused by repeated potassiation/depotassiation processes during cycling.[1-3] One promising class of anode materials for PIBs is transition-metal phosphides (TMPs), which provide a high specific capacity through conversion reactions, in addition to a relatively low voltage plateau.[4, 5] Unfortunately, TMPs are also plagued by large volume perturbations and an intrinsically low electrical conductivity, leading to rapid capacity fade during cycling and poor rate capability. To address both issues, carbon nanocomposites are being utilized, with notable performance enhancements being already achieved with sodium ion batteries (SIBs).[5-8] However, application of TMPs to PIBs is still at an early stage, with relatively few reports available.[4, 5] Guo *et al.* achieved a reversible capacity of 385 mAh g^{-1} at 50 mA g^{-1} for Sn_4P_3/C composite material, however, agglomeration of Sn_4P_3 nanoparticles after 50 cycles resulted in rapid capacity fading.[9] Later studies on GeP_5/C composites demonstrated improved cycling performance beyond 50 cycles.[10] Bai *et al.* fabricated CoP/N, P codoped carbon sheets which delivered a capacity of 127 mAh g^{-1} after 1000 cycles at 100 mA g^{-1}.[4]

Here we created Co_2P encapsulated in N-doped Carbon Cages "Co_2P@NCCs" for PIB anode application by a one-step carbonization and phosphidation of cobalt-imidazolate frameworks (ZIF-67). ZIF-67 were synthesized according to a previous report, albeit, without the addition of any surfactant.[11] **Fig. S1** shows the morphology of the as-synthesized ZIF-67 precursors. The method of fabricating Co_2P@NCCs is depicted in **Scheme 1.** The as-synthesized ZIF-67 nanocrystals were first activated under vacuum at 100°C overnight. Then the materials were ground with triphenylphosphine (PPh_3) in 1:1 wt. ratio in a glove box, followed by annealing at 900°C for 2h under Ar atmosphere. This yielded the Co_2P@NCC nanocomposites. The ZIF-67 served as a single solid precursor for cobalt, nitrogen and carbon, while PPh_3 was the source of phosphorus. Upon heating to 500-600°C, the organic linkers (2-methyimidazole) decomposed into nitrogen and cyano fragments, resulting in a local reducing atmosphere that transforms the Co^{2+} centers to metallic Co. Meanwhile the volatile carbon species condense on the Co particles resulting in a nanometer-thick carbon framework. In the presence of Co, PPh_3 will undergo an Ullmann-type reaction to yield the cobalt phosphide ($4Co + 2PPh_3 \rightarrow 2Co_2P + 3Ph\text{-}Ph$) nanoparticles.[12] The above strategy contrasts with the established "hot-injection method", which employs pyrophoric organophosphine as the phosphidation source, involves multi-step synthesis, and requires rigorous air-free conditions.[13] Other solid-state methods use $NaH_2PO_2/NH_4H_2PO_2$, which decomposes to yield toxic PH_3 as the "true" P precursor.[12]

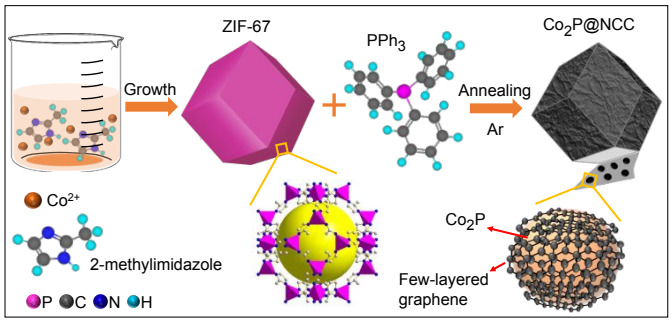

Scheme 1. Illustration of the fabrication process for obtaining Co_2P nanoparticles encapsulated N-doped carbon nanocages Co_2P@NCC.

[a] *Materials Research Centre, Indian Institute of Science, Bengaluru-560012, India.*
[b] *Department of Physics, Malaviya National Institute of Technology Jaipur, Rajasthan-302017, India.*
[c] *Chemical & Biomolecular Engineering and Mechanical Engineering, Clarkson University, Potsdam, New York 13699, USA.*
[d] *Materials Science and Engineering Program & Texas Materials Institute (TMI), The University of Texas at Austin, Austin, Texas-78712-1591, USA.*

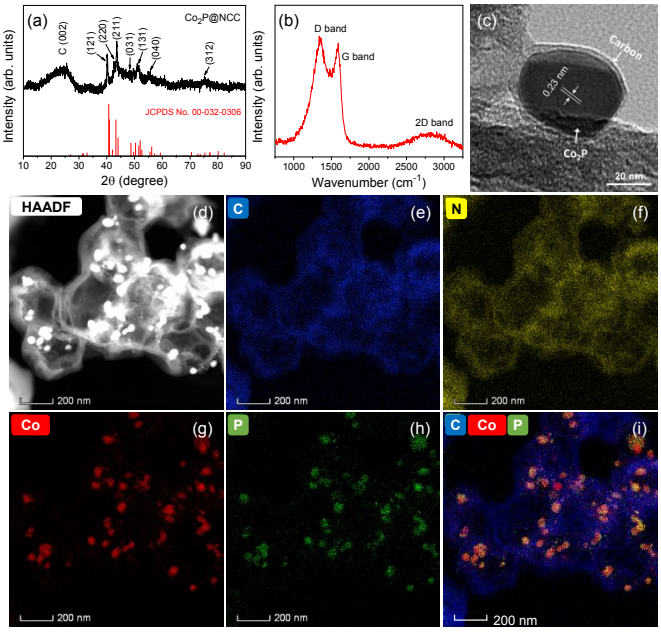

Fig. 1 (a) XRD pattern of Co_2P@NCC nanocomposite with major diffraction peaks indexed. (b) Raman spectrum of the nanocomposite showing the disordered structure of the carbon matrix per the relative D to G band intensity. (c) HRTEM image of a single Co_2P nanoparticle encapsulated by NCC. (d) HAADF-STEM image of the nanocomposite and (e)-(i) associated EELS elemental maps of C, N, Co, and P elements.

Fig. 1a shows the XRD pattern of the as-synthesized Co_2P@NCC. A broad peak centered around 25° corresponds to the (002) nearest neighbor positions of the carbon matrix. The major Bragg peaks are assigned to the orthorhombic Co_2P (JCPDS no. 32-0306).[14] The associated unit cell is shown in **Fig. S2.** The lack of other discernable crystalline peaks indicates high phase purity of the product.[5, 12] **Fig. 1b** shows the Raman spectrum recorded for Co_2P@NCCs. The spectrum shows two intense peaks at 1354 and 1591 cm^{-1} corresponding to D and G bands of the defective NCC.[6, 12, 15] The I_D/I_G ratio of Co_2P@NCCs is ~1, indicating that there are significant defects in the carbon framework, in part due to N heteroatom doping. **Fig. 1c** shows a HRTEM image of a single Co_2P nanoparticle encapsulated by NCC. The image shows aligned lattice fringes with interlayer separation of ~ 0.23 nm, corresponding to (121) crystalline planes of orthorhombic Co_2P, and in accordance with the XRD analysis. **Fig. 1d** shows the HAADF-STEM image of the nanocomposite, while **e-i** present the associated EELS elemental maps of C, N, Co, and P. Additional TEM and EELS analyses are shown in **Figs. S3** and **S4**. From the figures, it is evident that the N is uniformly doped into the carbon network. It may also be observed that the dark Co_2P nanoparticles are encapsulated inside the hollow carbon nanocages. This architecture was formed during the decomposition of MOFs in an inert atmosphere, as described earlier. The Co_2P nanoparticles are spherical in shape with an average size of 40 nm, as shown in **Fig. S5**. The Co_2P particles are preferentially attached to the edges of the carbon cages. This is due to the outward migration of the volatile species, in turn due to the decomposition of the organic linkers. The HRTEM image also reveals that the Co_2P nanoparticles are encapsulated by few layer-thick defective carbon.

Fig. S6a shows the core-level XPS survey spectrum of the Co_2P@NCC. **Fig. S6b** shows the high-resolution C 1s spectra which can be deconvoluted into four contributions centered at 284.4, 285.2, 287.0 and 290.0 eV, correspond to the sp^2-hybridized graphitic C, N-sp^2 C, N-sp^3 C, and $\pi \rightarrow \pi^*$ transitions.[5] Deconvolution of the N 1s spectrum (**Fig. S6c**) reveals the presence of pyridinic-N, pyrolic-N and graphitic-N centered around 398.4 eV, 400.0 eV and 401.8 eV, respectively.[12] These nitrogen functionalities will reversibly store additional K ions throughout the voltage range tested, as discussed below. In **Fig. S6d**, the core-level XPS spectrum of Co 2p shows two major peaks around binding energies of 780 and 795 eV, correspond to the Co $2p_{3/2}$ and Co $2p_{1/2}$ states, respectively.[5, 16] Upon deconvolution of Co $2p_{3/2}$ peak three distinct peaks could be observed with binding energies at 778.2, 781.2 and 785.7 eV, where the peak at binding energy 785.7 eV is the satellite of the peak at 781.2 eV. The peak at binding energy 778.2 eV indicates that there are reduced Co species in Co_2P. These reduced Co species are partially charged ($Co^{\delta+}$, $0<\delta<2$). The δ should have a small value as the corresponding Co $2p_{3/2}$ binding energy (778.2 eV) is close to the binding energy of metallic Co (777.9 eV).[14] With regard to the P 2p core-level spectrum (**Fig. S6e**), a doublet is observed at 129.6 eV and 131.0 eV. This can be attributed to the P $2p_{3/2}$ and P $2p_{1/2}$, respectively. The two subpeaks located around 133.5 eV and 134.5 eV are ascribed to P–C and P–O bonds. In accordance with the presence of partially charged $Co^{\delta+}$ species, the P 2p peak shifts negatively to 129.6 eV in comparison to elemental P (130.2 eV). This indicates the transfer of electron density from Co to P within the Co_2P structure.[12]

Figure 2 shows the electrochemical analysis results for Co_2P@NCC tested as a half-cell vs. K/K^+, in an electrolyte of 0.8 M KPF_6 in ethylene carbonate (EC) / diethyl carbonate (DEC) / propylene carbonate (PC) (2:1:2 vol/vol/vol) without any additives. Additional details of the testing protocol being provided in Supplemental. **Fig. 2a** shows the cyclic voltammetry (CV) measurements of initial five cycles of the Co_2P@NCC electrode at a scan rate of 0.1 mV s^{-1} within the voltage range of 0.01-3 V. The broad reduction peak appearing around 0.8 V in the first potassiation cycle is attributed to the formation of the solid electrolyte interphase (SEI).[5, 6] The broad reduction peak around 0.27 V is then assigned to the formation of K_3P, according to the reaction $Co_2P + 3K^+ + 3e^- \rightarrow 2Co + K_3P$.[6, 17] During the first anodic scan, the broadened oxidation peak between 0.34 V and 0.7 V is associated with the decomposition of K_3P according to the reaction $K_3P \rightarrow P + 3K^+ + 3e^-$.[6, 17] This reaction going opposite way is the source of the reversible capacity during subsequent potassiation. Metallic Co is not K active and Co_2P does not re-form upon depotassiation. From the second cycle onwards, the redox peaks are almost overlapping with each other, indicating stable potassiated and depotassiated microstructures.

The N-rich carbon host is an additional source of reversible K storage capacity, with the reversible ion adsorption and insertion mechanisms being analogous to the more widely studied Na storage.[1-3] Specifically, the K ions should reversibly bind to the N based moieties and to the structural defects associated with the heteroatoms and the graphene edge sites. There should also be limited reversible insertion of K into the bulk carbon lattice, although this capacity will be relatively minor due to the highly defective nature of the carbon host.[18] Since the reversible capacity reported here is based on the total mass of the anode, the contribution from the carbon host is accounted for.

The stable CV behavior agrees with the galvanostatic results, shown in **Fig. 2b**, for cycles 1 - 10 at a current density of 50 mA g^{-1}. Per the galvanostatic data, the cycle 1 Coulombic efficiency (CE) is 42%. This value agrees with prior results on K-based conversion systems, where CEs ranging from 19% to 57% have been reported.[4, 5, 19, 20] The density of Co_2P is 7.66 g cm^{-3}, that of K_3P is 1.70 g cm^{-3}, that of P is 1.82 g cm^{-3}, and that of Co is 8.86 g cm^{-3}. The specific volume of Co_2P is 0.130 cm^3 g^{-1}, that of K_3P is 0.588 cm^3 g^{-1}, that of P is 0.549 cm^3 g^{-1}, and that of Co is 0.112 cm^3 g^{-1}. Therefore, the volume change associated with the initial conversion of Co_2P to Co and K_3P is 0.57 cm^3 g^{-1}, which is 438%. The subsequent volume change associated the reversible conversion of K_3P to P is - 0.039 cm^3 g^{-1}, which is - 6.63%. It may be therefore concluded that at cycle 1 the volume changes are severe, while at subsequent cycles the volume changes are relatively mild. At cycle 1 there is expected to be some damage to the Co_2P@NCC structure, providing another source of CE loss in addition to the SEI. During cycling, however, the structure should be stable. The gradual increase in the long-term cycling capacity is likely an "activation" effect, where progressively more of the Co_2P phase becomes K-active. Moreover, there may be a contribution from the reversible formation and dissolution of a secondary polymeric SEI phase. Both effects are documented for Li and Na storage in cases when nanostructured conversion compounds are combined with carbon phases.[21]

The rate performance of Co_2P@NCC electrode was measured at current densities varying from 50-2000 mA g^{-1}, as shown in **Fig. 2c, d**. There continuously sloping plateaus in the potassiation/depotassiation profiles agree with what has been previously reported for conversion or alloying materials that are highly nanostructured.[5, 22] In such systems the depotassiated products are amorphized.[5] The material exhibits highly favorable depotassiation capacities of ~196, 155, 137, 113, and 91 mAh g^{-1}, at current densities of 100, 300, 500, 1000, and 2000 mA g^{-1}, respectively. Meanwhile, the steady-state CE approaches 100%. When the current density is reduced from 2000 mA g^{-1} back to 100 mA g^{-1}, 94% of the initial capacity is recovered.

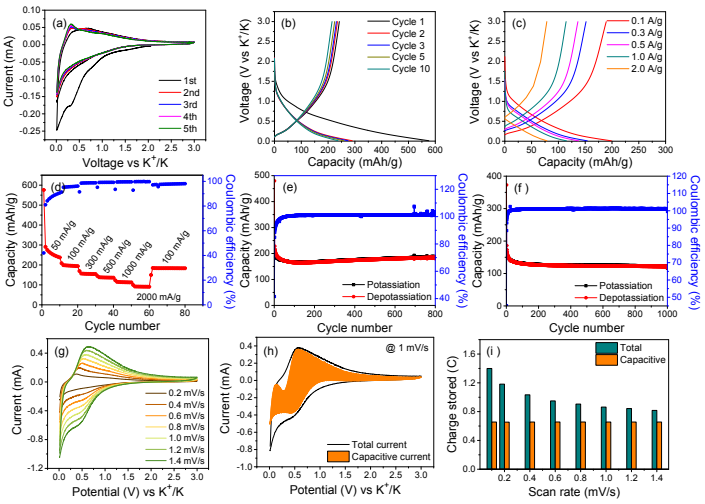

Fig. 2 Electrochemical analysis of Co_2P@NCC as KIB anode (a) CV data within 0.01-3 V vs. K/K^+, at 0.1 mV s^{-1}, (b) Cycle 1, 2, 3, 5 and 10 galvanostatic curves at 50 mA g^{-1}. (c) Cycle 10 galvanostatic curves at increasing current densities. (d) Rate performance of electrode material. (e) Cycling performance at 100 mA g^{-1}. (f) Cycling performance at 500 mA g^{-1}. (g) CVs at different scan rates. (h) Example of reaction-controlled (termed "Capacitive") and diffusion-controlled contributions at 1 mV s^{-1}, and (i) Capacitive vs. diffusion-controlled contribution ratios at scan rates from 0.1-1.4 mV s^{-1}.

As shown in **Fig. 2e**, the Co_2P@NCC anode shows early cycling capacity fade corresponding to a CE ~ 40%, again agreeing with prior literature on K-based anodes.[4, 5] However, there is minimal degradation from 10th to 800th cycle, with 96 % capacity retention. At cycle 800 the reversible capacity is around 190 mAh g^{-1}. The CE (shown on the right vertical axis) varies from 94.4% at 10th cycle to ~ 100% at 800th cycle. The constant shape of the associated galvanostatic profiles at cycles 10 - 800 (**Fig. S7)** support the conclusion about the stable microstructure. The Co_2P@NCC electrode also exhibits stable cycling performance at fast charge, as shown in **Fig. 2f**. After 1000 cycles at 500 mA g^{-1}, there is 82% retention of cycle 10 capacity and a steady-state cycling CE of ~ 100%. **Table S1** provides a detailed comparison of the rate performance of Co_2P@NCC versus state-of-the-art cobalt-based, phosphide-based, and carbon-based KIB anodes, indicating that the current system is among the best in terms of fast charge characteristics.[4, 5, 19, 20] Overall, the cycling performance of the Co_2P@NCC is favorable relative to other KIB conversion anodes reported in literature.[9, 23, 24]

The architecture of Co_2P@NCC offers several features that allow for its enhanced rate capability and cyclability. The single-nm scale carbon cage facilitates fast solid-state potassium ion diffusion and results enhanced electrical conductivity, while preventing the aggregation of active Co_2P nanoparticles. The carbon walls and the sub-40 nm average Co_2P diameter result in short solid-state ion diffusion pathways, necessary for fast kinetics. The presence of voids in the structure will help to accommodate the volume changes associated with the conversion reaction. It is known that N-rich carbons display promising specific capacities with K ions which would

be additive to the capacity of the reversible K_3P reaction.[5, 25] Since the reversible capacity calculated here is based on the total weight of the electrode, this contribution is accounted for. Nitrogen doping also enhances the electrical conductivity of carbon, while increasing the reversible capacity.[1-3] A high conductivity host will improve the rate capability of any ion active primary phase.[4] Benefitting from these features, the Co_2P@NCC electrode is demonstrated to be promising as an anode for potassium ion storage, especially at fast charging rates.

To gain further insight on the storage process in Co_2P@NCC, electrochemical reaction kinetics were analysed using CVs at different scan rates, per **Fig. 2g**. The charge storage kinetics can be separated into reaction-controlled versus diffusion-controlled, with the relative contributions varying with the scan rate. The current (*i*) in a cyclic voltammogram and scan rate (*v*) will obey the mathematical relation $i(V) = a_1 v + a_2 v^{1/2}$.[26-28] The total current is the sum of reaction-controlled currents ($a_1 v$) and diffusion-controlled currents ($a_2 v^{1/2}$). Here the reaction-controlled process is termed "Capacitive", agreeing with common literature designation.[29, 30] **Fig. 2h** shows the capacitive versus diffusion-controlled contribution at 1 mV s^{-1}, indicates the dominance of the former. The two relative contributions are plotted **Fig. 2i** for scan rates of 0.1 to 1.4 mV/s. A gradual increase in the relative capacitive contribution towards total charge storage capacity occurs with increasing scan rates: the capacitive contribution is 47%, 55.3%, 63.5%, 69.2%, 72.5%, 76%, 77.6%, and 80.3% at 0.1, 0.2, 0.4, 0.6, 0.8, 1.0, 1.2, and 1.4 mV/s, respectively. The capacitive contributions in Co_2P@NCC is higher than in prior reports, indicative of its fast reaction kinetics.[31-34]

D.S. was supported by Department of Science and Technology, Government of India, through Inspire Faculty Award (IFA-14 MS-32), and Science & Engineering Research Board (SERB), Government of India, through the project SRG/2019/001211. D.D. acknowledges Royal Society of Chemistry for an Early Career Researcher Mobility Grant (Grant no. 308812). D.M. (conception and guidance of research, preparation of manuscript) was supported by the National Science Foundation, Civil, Mechanical and Manufacturing Innovation (CMMI), Award Number 1911905.

Conflicts of interest:

There are no conflicts to declare.

References

1. N. Yabuuchi, K. Kubota, M. Dahbi and S. Komaba, *Chem. Rev.*, 2014, **114**, 11636-11682.
2. C. Bommier, D. Mitlin and X. Ji, *Prog. Mater. Sci.*, 2018, **97**, 170-203.
3. T. Hosaka, K. Kubota, A. S. Hameed and S. Komaba, *Chem. Rev.*, 2020, **120**, 6358-6466.
4. J. Bai, B. Xi, H. Mao, Y. Lin, X. Ma, J. Feng and S. Xiong, *Adv. Mater.*, 2018, **30**, 1802310.
5. Y. Wang, Z. Zhang, G. Wang, X. Yang, Y. Sui, F. Du and B. Zou, *Nanoscale Horiz.*, 2019, **4**, 1394-1401.
6. D. Zhou and L.-Z. Fan, *J. Mater. Chem. A*, 2018, **6**, 2139-2147.
7. Q. Liu, L. Fan, R. Ma, S. Chen, X. Yu, H. Yang, Y. Xie, X. Han and B. Lu, *Chem. Commun.*, 2018, **54**, 11773-11776.
8. C. Dong, L. Guo, Y. He, C. Chen, Y. Qian, Y. Chen and L. Xu, *Energy Storage Mater.*, 2018, **15**, 234-241.
9. W. Zhang, J. Mao, S. Li, Z. Chen and Z. Guo, *J. Am. Chem. Soc.*, 2017, **139**, 3316-3319.
10. W. Zhang, Z. Wu, J. Zhang, G. Liu, N.-H. Yang, R.-S. Liu, W. K. Pang, W. Li and Z. Guo, *Nano Energy*, 2018, **53**, 967-974.
11. H. Hu, Bu Y. Guan and Xiong W. Lou, *Chem*, 2016, **1**, 102-113.
12. D. Das, A. Das, M. Reghunath and K. K. Nanda, *Green Chem.*, 2017, **19**, 1327-1335.
13. S. Carenco, Y. Hu, I. Florea, O. Ersen, C. Boissière, N. Mézailles and C. Sanchez, *Chem. Mater.*, 2012, **24**, 4134-4145.
14. Z. Huang, Z. Chen, Z. Chen, C. Lv, M. G. Humphrey and C. Zhang, *Nano Energy*, 2014, **9**, 373-382.
15. A. Kumar, D. Das, D. Sarkar, S. Patil and A. Shukla, *J. Electrochem. Soc.*, 2020, **167**, 060529.
16. A. K. Singh and D. Sarkar, *J. Mater. Chem. A*, 2017, **5**, 21715-21725.
17. W. Miao, X. Zhao, R. Wang, Y. Liu, L. Li, Z. Zhang and W. Zhang, *J. Colloid Interface Sci.*, 2019, **556**, 432-440.
18. Z. Xu, M. Wu, Z. Chen, C. Chen, J. Yang, T. Feng, E. Paek and D. Mitlin, *Adv. Sci.*, 2019, **6**, 1802272.
19. X. Wang, J. Ma, J. Wang and X. Li, *J. Alloys Compd.*, 2020, **821**, 153268.
20. X. Zhao, W. Wang, Z. Hou, G. Wei, Y. Yu, J. Zhang and Z. Quan, *Chem. Eng. J.*, 2019, **370**, 677-683.
21. J. Ding, W. Hu, E. Paek and D. Mitlin, *Chem. Rev.*, 2018, **118**, 6457-6498.
22. S.-B. Son, L. Cao, T. Yoon, A. Cresce, S. E. Hafner, J. Liu, M. Groner, K. Xu and C. Ban, *Adv. Sci.*, 2019, **6**, 1801007.
23. H. Gao, T. Zhou, Y. Zheng, Q. Zhang, Y. Liu, J. Chen, H. Liu and Z. Guo, *Adv. Funct. Mater.*, 2017, **27**, 1702634.
24. V. Lakshmi, Y. Chen, A. A. Mikhaylov, A. G. Medvedev, I. Sultana, M. M. Rahman, O. Lev, P. V. Prikhodchenko and A. M. Glushenkov, *Chem. Commun.*, 2017, **53**, 8272-8275.
25. Y. Zhang, A. Pan, L. Ding, Z. Zhou, Y. Wang, S. Niu, S. Liang and G. Cao, *ACS Appl. Mater. Interfaces*, 2017, **9**, 3624-3633.
26. D. Sarkar, D. Das, S. Das, A. Kumar, S. Patil, K. K. Nanda, D. D. Sarma and A. Shukla, *ACS Energy Lett.*, 2019, **4**, 1602-1609.
27. D. Chao, C. Zhu, P. Yang, X. Xia, J. Liu, J. Wang, X. Fan, S. V. Savilov, J. Lin, H. J. Fan and Z. X. Shen, *Nat. Commun.*, 2016, **7**, 12122.
28. B. Lee, M. Kim, S. Kim, J. Nanda, S. J. Kwon, H. D. Jang, D. Mitlin and S. W. Lee, *Adv. Energy Mater.*, 2020, **10**, 1903280.
29. J. Wang, J. Polleux, J. Lim and B. Dunn, *J. Phys. Chem. C*, 2007, **111**, 14925-14931.
30. T. Brezesinski, J. Wang, S. H. Tolbert and B. Dunn, *Nature Mater.*, 2010, **9**, 146-151.
31. J. Liao, Q. Hu, J. Mu, F. Chen, X. He, F. Chen, Z. Wen and C. Chen, *Chem. Commun.*, 2020, **56**, 8392-8395.
32. P. Xiao, S. Li, C. Yu, Y. Wang and Y. Xu, *ACS Nano*, 2020, **14**, 10210-10218.
33. Y. Liu, K. Cui, Z. Ma and X. Wang, *Energy Fuels*, 2020, **34**, 10196-10202.
34. X. Shi, L. Qin, G. Xu, S. Guo, S. Ma, Y. Zhao, J. Zhou and S. Liang, *Chem. Commun.*, 2020, **56**, 3713-3716.

Co_2P nanoparticles encapsulated in N-doped carbon nanocages (Co_2P@NCCs) as Potassium ion battery anodes with state-of-the-art electrochemical performance.